

## Gyrokinetic Particle Simulation of Compressional Electromagnetic Modes

H. Qu and Z. Lin\*

*Department of Physics and Astronomy, University of California, Irvine, CA 92697, USA.*

Received 7 November 2007; Accepted (in revised version) 20 December 2007

Available online 14 April 2008

---

**Abstract.** A gyrokinetic particle simulation model is developed for simulations of the compressional electromagnetic turbulence driven by the mirror instability. Results of the linear simulations of mirror modes agree well with the analytic dispersion relation. Nonlinear simulations of a single mode find that the mirror instability saturates via a phase-space trapping due to the nonlinear wave-particle interaction when the instability drive is weak.

**PACS (2006):** 52.30.Gz, 52.35.Hr, 52.35.Mw, 52.35.Py, 52.65.Rr, 52.65.Tt

**Key words:** Mirror instability, compressional electromagnetic turbulence, particle-in-cell simulation.

---

### 1 Introduction

The gyrokinetic particle simulation [1] is very popular for studying the electrostatic modes [2] or incompressible shear Alfvén waves [3, 4]. The extension of the gyrokinetic particle simulation to compressible modes, such as mirror instability, could be useful. The mirror instability is a low frequency electromagnetic mode destabilized by the pressure anisotropy in plasmas with high- $\beta$  ( $\beta = 8\pi P / B^2$ , the ratio between kinetic and magnetic pressure). It has long been studied in space plasmas, such as planetary and cometary magnetosheaths, in which the velocity distribution of charged particles can deviate substantially from the canonical Maxwellian distribution because collisions occur very rarely. In such environments, the pressure anisotropy can give rise to the excitation of collective modes. Particularly, when the perpendicular temperature exceeds the parallel temperature i.e.,  $T_{\perp} > T_{\parallel}$ , a magnetic mirror instability at very low frequencies  $\omega \ll k_{\parallel} v_i$  can occur ( $v_i$  is the ion thermal velocity and  $k_{\parallel}$  is the wave vector parallel to the magnetic field).

---

\*Corresponding author. *Email address:* hqu@uci.edu (H. Qu), zhihong1@uci.edu (Z. Lin)

Here and in the rest of the article, subscripts  $\parallel$  and  $\perp$  correspond to B-parallel and perpendicular components respectively). This instability has attracted considerable interest because of its probable importance in the contribution to the low-frequency compressible magnetic turbulence in magnetized plasmas.

Much attention has been paid to the theoretical analysis of the mirror mode under various conditions [5–10]. A discussion of the physical mechanism of the linear mirror instability in the cold electron temperature limit (i.e.,  $T_{e,\parallel} \sim T_{e,\perp} \ll T_{i,\parallel}$ ) was offered by *Southwood* and *Kivelson* [11]. The authors showed that the mirror instability results from a resonant interaction between ions with small parallel velocities and low frequency electromagnetic fluctuations. The nonlinear evolution of the mirror instability has also been studied by *Kivelson*, *Southwood* and *Pantellini* [12, 13]. The linear theories in the long wavelength limit find that the linear growth rate of the mirror instability increases with  $k_{\perp}$ . Therefore, it is obvious that the finite Larmor radius (FLR) effects can play an important role when the perpendicular wavelength becomes comparable to the ion gyroradius. In fact, some observations in the Earth magnetosphere [14–20] and the Jovian magnetosheath [21, 22] revealed evidence for the presence of such short perpendicular wavelengths. Thus, in some papers [8, 10, 23–25], the FLR effects on the mirror mode were considered. Nonetheless, it is desirable to develop a kinetic theory with a transparent physics picture that also provides an efficient tool for nonlinear studies of the mirror instability, both analytically and computationally. Here we adopt the gyrokinetic theory [26, 27] instead of the Vlasov theory. The gyrokinetic theory is a powerful approach for the nonlinear analysis and simulation of the low-frequency instabilities. It employs the gyrokinetic ordering that the characteristic frequency of wave and the gyroradius are small compared with the gyro-frequency and unperturbed scale length, respectively, and that the perturbed parallel scale lengths are of the order of the unperturbed scale lengths. Such an ordering enables us to get rid of the explicit dependence of the Vlasov equation on the gyrophase angle while retaining the FLR effects and the nonlinear dynamics.

A gyrokinetic particle-in-cell (PIC) simulation for the compressible mirror mode [28] has been developed and applied for the study of the mirror instability in this work. This is the first time that gyrokinetic particle model is extended to treat the compressional electromagnetic modes. Among the various methods used in the plasma simulation, particle simulation is promising. Numerical PIC simulation has proven to be a powerful tool in understanding the kinetic physics of various fundamental plasma processes, especially where the plasma dynamics is of nonlinear nature under realistic conditions. However, the PIC simulation also has its share of limitations. For example, in the conventional PIC models, many high frequency modes can be produced. It is generally agreed that conventional PIC models are not efficient for studying the low-frequency phenomena, because of the disparate time and spatial scales involved. Motivated by the inadequacy in the existing simulation models, we extend the gyrokinetic PIC simulation model [1] for the mirror mode, in which the rapid gyromotion is removed through gyroaveraging while the vital FLR effects and nonlinear dynamics are retained. By eliminating the gyromotion of particles, we can remove the high frequency modes and use much larger time steps to

save the computation power. The gyrokinetic simulation PIC model is particularly suitable for the mirror instability with wave frequency  $\omega \ll \Omega_i$ .

The paper is organized as follows. Section 2 describes the basic gyrokinetic Vlasov-Maxwell equations for the particle simulation and some basic numerical schemes. Section 3 shows the linear benchmark. Section 4 discusses some nonlinear simulation results and the saturation mechanism of the mirror instability. Section 5 is the summary of our work.

## 2 Gyrokinetic particle simulation of compressional modes

As discussed in Section 1, we are interested in the low frequency (i.e.,  $\omega/\Omega_i \ll 1$ ) and short wavelength (i.e.,  $k_\perp \rho_i \sim 1$ ) mirror instability, it satisfies the following gyrokinetic orderings [26,27]

$$\begin{aligned} \frac{\omega}{\Omega_i} \sim \frac{\rho_i}{L} \sim k_\parallel \rho_i \sim \frac{\delta B}{B} \sim \varepsilon \\ k_\perp \rho_i \sim 1. \end{aligned} \quad (2.1)$$

Here,  $\Omega_i = qB_0/m_i c$  and  $\rho_i = v_{i,\perp}/\Omega_i$  are, respectively, the ion cyclotron frequency and Larmor radius,  $L$  is the macroscopic background plasma scale length,  $k_\parallel$  and  $k_\perp$  are the parallel and perpendicular wave vectors,  $\delta B$  and  $B$  are the perturbed and total magnetic field, and  $\varepsilon$  is the smallness parameter.

### 2.1 Gyrokinetic Vlasov-Maxwell equations

The common and distinctive property of the mirror instability is its low frequency. The gyrokinetic equations are the equations that exploit this property. It reduces the Vlasov-Maxwell equations by averaging the fast gyration while the FLR effects and the nonlinear dynamics are retained to analyze the low frequency plasma dynamics [27].

The reduced system has been obtained through the use of gyrokinetic ordering Eq. (2.1). Here, for the nonlinear simulation, we use the so-called gyrocenter coordinates instead of the guiding-center coordinates [27]. In the absence of the perturbed electromagnetic fields, the gyrocenter coordinates are reduced to the guiding-center coordinates. The introduction of the electromagnetic perturbation results in the reintroduction of the gyroangle dependence to the guiding-center Hamiltonian, and consequently the magnetic moment  $\mu = v_\perp^2/2B_0$  is no longer an invariant. Thus, a new set of gyrocenter Hamiltonian equations are needed through the elimination of the gyroangle dependence from the perturbed guiding-center equations. This provides a transformation from the guiding-center coordinates to the gyrocenter coordinates  $(\bar{\mathbf{X}}, \bar{\rho}_\parallel, \bar{\mu}, \bar{\zeta})$ , where  $\bar{\mathbf{X}}$  is the gyrocenter position,  $\bar{\rho}_\parallel = \bar{U}/\Omega$ ,  $\bar{U}$  is the gyrocenter parallel velocity,  $\bar{\mu} = \bar{v}_\perp^2/2B$  is the adiabatic invariant,  $\mathbf{B} = \mathbf{B}_0 + \delta\mathbf{B}$ ,  $\bar{\zeta}$  is the gyrophase angle [27].

When  $T_e/T_i \ll 1$ , the kinetic effects of electrons on mirror instability can be neglected. Therefore, the gyrokinetic simulation model is developed in this limit by only treating

ions with the gyrokinetic model. The following gyrokinetic equation can be obtained by averaging the Vlasov equation over the gyrophase angle [27]

$$\frac{\partial F_i}{\partial t} + (\bar{\mathbf{U}}\mathbf{b} + \dot{\bar{\mathbf{X}}}_\perp) \cdot \nabla F_i + \dot{\bar{\rho}}_\parallel \frac{\partial F_i}{\partial \bar{\rho}_\parallel} = 0,$$

where  $F_i(\bar{\mathbf{X}}, \bar{\rho}_\parallel, \bar{\mu})$  is the gyrocenter distribution function of ions in the reduced five-dimensional gyrocenter phase space. To reduce the level of the particle noise, we use the  $\delta f$  method [32,33]. Let

$$F_i = F_{0i} + \delta F_i,$$

where  $F_{0i}$  and  $\delta F_i$  are the equilibrium and the perturbed distribution functions of ions, respectively. Then, in the uniform plasma and equilibrium magnetic field, the gyrokinetic Vlasov equation for the perturbed distribution function can be written as

$$\frac{\partial \delta F_i}{\partial t} + (\bar{\mathbf{U}}\mathbf{b} + \dot{\bar{\mathbf{X}}}_\perp) \cdot \nabla \delta F_i + \dot{\bar{\rho}}_\parallel \frac{\partial \delta F_i}{\partial \bar{\rho}_\parallel} = -\dot{\bar{\rho}}_\parallel \frac{\partial F_{0i}}{\partial \bar{\rho}_\parallel} \quad (2.2)$$

and the equations of motion for ions in Eq. (2.2) are

$$\frac{d\bar{\mathbf{X}}_\parallel}{dt} = \bar{\mathbf{U}} = \bar{\rho}_\parallel \Omega_i, \quad (2.3)$$

$$\frac{d\bar{\mathbf{X}}_\perp}{dt} = \frac{c}{B_0} \mathbf{b} \times \nabla \langle \delta \varphi - \frac{1}{c} \mathbf{v} \cdot \delta \mathbf{A} \rangle, \quad (2.4)$$

$$\dot{\bar{\rho}}_\parallel = \frac{\bar{\mathbf{U}}}{\Omega_i} = -\frac{q}{\Omega_i m} \mathbf{b} \cdot \nabla \langle \delta \varphi - \frac{1}{c} \mathbf{v} \cdot \delta \mathbf{A} \rangle, \quad (2.5)$$

where

$$\langle \dots \rangle = \frac{1}{2\pi} \int_0^{2\pi} (\dots) d\zeta$$

represents gyro-averaging. Here,  $\delta \varphi$  and  $\delta \mathbf{A}$  are the perturbed scalar and vector potentials, respectively. In the gyrokinetic simulation, the gyro-averaging can be carried out numerically on a discretized gyro-orbit in real space (see Section 2.2).

In order to advance  $\delta F_i$ , we need to calculate  $\delta \varphi$ ,  $\delta A_\parallel = \mathbf{b} \cdot \delta \mathbf{A}$  and  $\delta B_\parallel = i(\mathbf{b} \times \mathbf{k}_\perp) \cdot \delta \mathbf{A}$  from Poisson equation and Ampere's law. It is straightforward to include the contribution from  $\delta A_\parallel$  and  $\delta \varphi$ . Here, because the mirror instability is dominated by the contribution of  $\delta B_\parallel$ , to focus on the nonlinear physics of the mirror instability, we keep only the perpendicular Ampere's law for simplification. In the case of the Bi-Maxwellian velocity distribution, the perpendicular Ampere's law can be expressed as [28–30]

$$-\frac{i\delta j_{y0}}{ck_\perp} + \frac{\delta B_\parallel}{4\pi} = -\frac{k_\parallel^2}{k_\perp^2} [1 + \alpha_b \cdot (\beta_\perp - \beta_\parallel)] \frac{\delta B_\parallel}{4\pi}, \quad (2.6)$$

$$\delta j_{y0} = q_i \int v_y \delta F_i d\mathbf{v} + i\delta B_\parallel \frac{2nT_{i,\perp}ck_\perp}{B_0^2} e^{-k_\perp^2 \rho_i^2 / 2} [I_0(k_\perp^2 \rho_i^2 / 2) - I_1(k_\perp^2 \rho_i^2 / 2)], \quad (2.7)$$

where

$$\alpha_b = \int_{-\infty}^{+\infty} dv_{\parallel} \int_0^{+\infty} v_{\perp} dv_{\perp} \cdot 4\pi \frac{q^2}{m} \frac{\partial F}{B \partial \mu} \frac{v_{\parallel}^2 v_{\perp}^2}{\Omega^2 c^2} (J_1')^2,$$

$I_0$  and  $I_1$  are the modified Bessel functions. Here, the second term on the right side of Eq. (2.7) comes from the perpendicular gyrocenter drift.

Gyrokinetic equation of perturbed distribution function Eq. (2.2), equations of motion Eqs. (2.3)-(2.5) and field equation Eq. (2.6) form a complete set of the gyrokinetic Vlasov-Maxwell equations for the simulation.

## 2.2 Numerical methods

Over the years, the computational community has developed many methods used in the numerical simulation. Here are some basic schemes used in our gyrokinetic PIC simulation of the compressional modes.

### 2.2.1 Finite size particle

In real plasmas, charged particles move according to the electromagnetic field acting on them, as do the particles in the computational plasma. To illustrate this idea, we can start from the gyrokinetic equation Eq. (2.2) and the equations of motion Eqs. (2.3)-(2.5). Obviously, to get the characteristics of particles, the gyrokinetic equation needs to be closed by the Maxwell equations, i.e., Eq. (2.6) for  $\delta B_{\parallel}$ , the Poisson equation for  $\delta \varphi$  and the parallel Ampere's law for  $\delta A_{\parallel}$ .

In the PIC simulation, the space is divided into small "cells" where only on the center of the cells (grids), the electromagnetic fields are known. Therefore,  $\delta B_{\parallel}$ ,  $\delta \varphi$  and  $\delta A_{\parallel}$  are calculated via charge and current densities on the spatial grids, the charge and current densities are calculated straightforwardly from the particles nearby the grids while the meaning "nearby" needs a precise definition. Simply, the charge and current densities are obtained from the appropriate moments of distribution function, i.e. [1],

$$\begin{aligned} \rho(\mathbf{x}_m) &= q \int f(\mathbf{x}_m) d\mathbf{v} = q \left\langle \sum_n \delta \langle \bar{\mathbf{X}}_m - \bar{\mathbf{X}}_n \rangle \right\rangle, \\ \mathbf{j}(\mathbf{x}_m) &= q \int \mathbf{v} f(\mathbf{x}_m) d\mathbf{v} = q \left\langle \mathbf{v} \sum_n \delta \langle \bar{\mathbf{X}}_m - \bar{\mathbf{X}}_n \rangle \right\rangle, \end{aligned}$$

where  $m$  and  $n$  are grid and particle indices,  $\mathbf{x} = \mathbf{X} - \rho = \mathbf{X} - \mathbf{v} \times \mathbf{e}_{\parallel} / \Omega$ ,  $\langle \dots \rangle = \frac{1}{2\pi} \int_0^{2\pi} (\dots) d\zeta$  represents the gyroaveraging. Then, applying the calculated charge and current density, we can find the electromagnetic fields on the corresponding grid points. When it comes to determining the motion of particles, we need the microscopic fields acting on the indi-

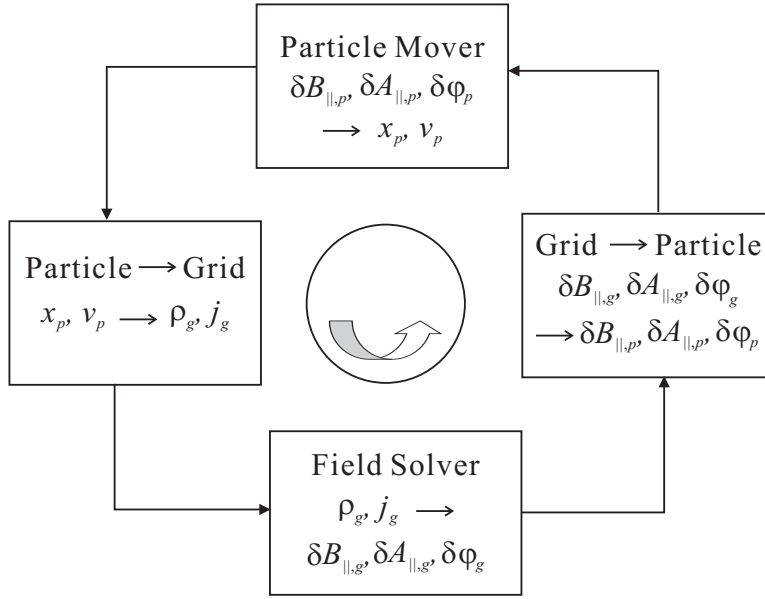


Figure 1: Steps in the cycle of PIC simulation. Subscripts  $p$  and  $g$  indicate particle and grid, respectively.

vidual particle at the gyrocenter of that particle. They can be determined as

$$\begin{aligned} \langle \delta\varphi(\mathbf{x}_n) \rangle &= \langle \int \delta\varphi(\mathbf{x}) \delta(\mathbf{x} - \mathbf{x}_n) d\mathbf{x} \rangle = \langle \sum_m \delta\varphi(\bar{\mathbf{X}}_m) \delta(\bar{\mathbf{X}}_m - \bar{\mathbf{X}}_n) \rangle, \\ \langle \delta\mathbf{A}(\mathbf{x}_n) \rangle &= \langle \int \delta\mathbf{A}(\mathbf{x}) \delta(\mathbf{x} - \mathbf{x}_n) d\mathbf{x} \rangle = \langle \sum_m \delta\mathbf{A}(\bar{\mathbf{X}}_m) \delta(\bar{\mathbf{X}}_m - \bar{\mathbf{X}}_n) \rangle. \end{aligned}$$

Therefore, there are two steps involved in the PIC simulation. These two steps form a complete computational circle to self-consistently calculate the wave and particle dynamics. Fig. 1 shows the computational circle.

To be more specific, we need to define the way of gathering the particles to the grids and scattering fields on the grids to the particles, i.e., to define precisely what is "nearby". The simplest way is to add together the particles in the same cell defined by the grids, and disregard all other particles. Because this scheme counts the contribution of particles in the nearest cell, it is called "nearest-grid-point" (NGP). Then, the densities on the grids can be written as

$$\rho(\mathbf{x}_m) = q \langle \sum_n S(\bar{\mathbf{X}}_m - \bar{\mathbf{X}}_n) \rangle, \quad \mathbf{j}(\mathbf{x}_m) = q \langle \mathbf{v} \sum_n S(\bar{\mathbf{X}}_m - \bar{\mathbf{X}}_n) \rangle,$$

where the  $\delta$ -function is replaced by the shape function for NGP as

$$S(x) = \begin{cases} 0 & |x| > \Delta x/2, \\ 1 & |x| < \Delta x/2. \end{cases}$$

Here,  $\Delta x$  is the grid size. Accordingly,

$$\langle \delta\varphi(\mathbf{x}_n) \rangle = \langle \sum_m \delta\varphi(\bar{\mathbf{X}}_m) S(\bar{\mathbf{X}}_m - \bar{\mathbf{X}}_n) \rangle, \quad \langle \delta\mathbf{A}(\mathbf{x}_n) \rangle = \langle \sum_m \delta\mathbf{A}(\bar{\mathbf{X}}_m) S(\bar{\mathbf{X}}_m - \bar{\mathbf{X}}_n) \rangle.$$

Due to the noisy behavior of NGP, many other options for the shape function were proposed [31]. In our simulation, we use the linear interpolation function,

$$S(x_m - x_n) = \max \left[ 0, 1 - \frac{|x_m - x_n|}{\Delta x} \right].$$

### 2.2.2 Gyroaveraging

In the gyrokinetic PIC simulation, the important dynamics is the motion of the gyrocenter instead of the charged particle. Thus, we need to introduce the scheme of the gyroaveraging to simplify the study analytically and numerically. There are two possible ways to do the gyroaveraging. One is to utilize the Fourier transformation which is directly connected to the analytical formulation, the other is the multi-points averaging on a charged ring [1].

The operation of gyroaveraging involves the transformation  $\mathbf{x} = \mathbf{X} - \rho = \mathbf{X} - \mathbf{v} \times \mathbf{e}_{\parallel} / \Omega$ . Firstly, to see the gyroaveraging operation via Fourier transformation, we know

$$P(\mathbf{x}) = \sum_k P_k e^{i\mathbf{k} \cdot \mathbf{x}} = \sum_k P_{gk} e^{i\mathbf{k} \cdot \mathbf{X}},$$

where  $P$  is a physical quantity,  $P_k$  and  $P_{gk}$  are its Fourier component in  $\mathbf{x}$  and  $\mathbf{X}$  space. It means we are writing  $P(\mathbf{x})$  in two different Fourier sums, with  $P_k$  and  $P_{gk}$  being the corresponding coefficients. Using this relation and the relation of  $\mathbf{x}$  and  $\mathbf{X}$ , we know  $P_k = P_{kg} e^{i\mathbf{k} \cdot \rho}$  or  $P_{kg} = P_k e^{-i\mathbf{k} \cdot \rho}$ . Now considering the particle motion is a periodic gyromotion, we can express  $P_{gk}$  as

$$P_{gk} = \sum_{n=-\infty}^{+\infty} \langle P_{gk} \rangle_n e^{-in\alpha},$$

where

$$\langle P_{gk} \rangle_n = (2\pi)^{-1} \int P_{gk} e^{in\alpha} d\zeta.$$

Since

$$e^{i\mathbf{k} \cdot \rho} = e^{-ik_{\perp} \rho \sin\alpha} = \sum_{n=-\infty}^{+\infty} J_n(k_{\perp} \rho) e^{-in\alpha},$$

we get

$$\langle P_{gk} \rangle = J_0(\lambda) P_k,$$

where  $\langle \dots \rangle = 1/2\pi \int_0^{2\pi} (\dots) d\zeta$ . This shows that, to perform gyroaveraging on a physical quantity, is equivalent to multiply a factor of Bessel function to its Fourier transform.

However, since the calculation of Bessel function for each individual particle to account for its interaction with all waves in the system is computational prohibitive, the

alternative multi-points averaging scheme is developed [1]. The basic idea is to treat the charged particle as a uniformly charged ring with its center located at the guiding-center and with a gyroradius  $\rho$ . For the particle whose guiding-center at  $\mathbf{X}$ , the charge is equally distributed at  $M$  locations of  $x$ 's on the ring. We know

$$P(\mathbf{X}) = \langle P(\mathbf{x}) \rangle = \left\langle \sum_k P_k e^{i\mathbf{k} \cdot (\mathbf{x} + \rho)} \right\rangle = \sum_k P_k J_0(\lambda) e^{i\mathbf{k} \cdot \mathbf{X}}.$$

To get the accurate representation of gyroaveraging, it is important to determine the optimal number of points (locations) on a ring, because it directly affects the computational time and viability of the scheme. One way to solve this problem is to study the numerical integration of

$$\begin{aligned} \langle \exp(i\mathbf{k} \cdot \rho) \rangle &= (2\pi)^{-1} \int_{-\pi}^{\pi} \exp(i\mathbf{k} \cdot \rho) e^{in\alpha} d\alpha \\ &= \sum_{n=-\infty}^{+\infty} J_n(\lambda) \sum_{l=1}^M \exp(i2\pi nl/M) / M, \end{aligned}$$

where  $M$  is the number of integration steps. Obviously, integration is more accurate when  $M$  is larger, but it is undesirable. Since  $J_0 \gg J_4$  for  $\lambda = k_{\perp} \rho < 2$ ,  $M=4$  or  $8$  is adequate in many applications.

### 2.2.3 $\delta f$ scheme

The basic idea of the  $\delta f$  scheme is to separate the particle distribution function into the equilibrium and the perturbed parts, and to use the particles to represent the perturbed part only. By doing so, we can reduce the particle noise associated with the equilibrium distribution and thus the number of particles required to a successful simulation can be greatly reduced [32,33].

We begin by writing distribution function as  $f = F_0 + \delta f$ , where  $F_0$  is the equilibrium background distribution and  $\delta f$  is the perturbed time-dependent part of the distribution function. Substitute  $f$  to the gyrokinetic equation, in the uniform plasma and magnetic field, we get the gyrokinetic equation for the perturbed distribution function as Eq. (2.2). In the PIC simulation, to solve this equation, we may consider loading a large number of particles to sample the phase space. We can define "particle weight" as

$$w_n \equiv \frac{\delta f}{f},$$

where  $n$  shows particle indices. Accordingly,  $\delta f$  can be represented as

$$\delta f(\mathbf{x}, \mathbf{v}, t) = \sum_{n=1}^N w_n S(\mathbf{x} - \mathbf{x}_n) \delta(\mathbf{v} - \mathbf{v}_n),$$

where  $S$  is the particle shape function. By taking the total time derivative of gyrokinetic equation, we obtain

$$\dot{w}_n = -\dot{\rho}_{\parallel} \frac{\partial F_0}{F_0 \partial \rho_{\parallel}}. \quad (2.8)$$

Here, we have already assumed a given equilibrium distribution of particles. Therefore, we need to initially load the correct particle equilibrium distribution function to ensure the correct  $\delta f$  calculation in the simulation.

#### 2.2.4 Initial loading

We begin with the simplest uniform distribution. To load the particle uniformly, we only need a random number generator which can generate the position of particles in phase space. After getting the uniform distribution

$$p(x)dx = \begin{cases} dx & 0 < x < 1, \\ 0 & \text{otherwise} \end{cases}$$

according to the fundamental transformation law of probabilities,

$$|p(y)dy| = |p(x)dx|,$$

we can get other distribution  $p(y)$  from the uniform distribution  $p(x)$ , with the help of the so-called "cumulative distribution function"  $y(x)$ , which is simply solved by [34].

$$p(y)dy = \left| \frac{dx}{dy} \right| dy.$$

For a number  $x_i$  generated by uniform random generator, the number  $y(x_i)$  is the corresponding one for distribution  $p(y)$ . As an example, taking  $y(x) = -\ln(x)$ ,

$$p(y)dy = \left| \frac{dx}{dy} \right| dy = e^{-y} dy$$

is distributed exponentially.

This method can also be generalized to a multi-dimensional distribution function [34],

$$p(y_1, y_2, \dots) dy_1 dy_2 \dots = \left| \frac{\partial(x_1, x_2, \dots)}{\partial(y_1, y_2, \dots)} \right| dy_1 dy_2 \dots,$$

where  $|\partial(\dots)/\partial(\dots)|$  is the Jacobian determinant. An important example of the use of this equation is the *Box-Muller* method for generating random deviates with a Maxwellian distribution

$$p(y)dy = \frac{1}{\sqrt{2\pi}} e^{-y^2/2} dy.$$

Considering the transformation between two uniform deviates on  $(0,1)$ ,  $x_1$ ,  $x_2$  and two quantities  $y_1$ ,  $y_2$  we have

$$\begin{cases} y_1 = \sqrt{-2\ln(x_1)}\cos(2\pi x_2), \\ y_2 = \sqrt{-2\ln(x_1)}\sin(2\pi x_1). \end{cases}$$

### 2.2.5 Integration of particle orbit and numerical stability

We now consider the scheme for time integration. Here, we adopt a very general and simple method, the 2<sup>nd</sup> order Runge-Kutta method. To present it more clearly, let us consider the following set of differential equations of an oscillator:

$$\begin{cases} \frac{dx}{dt} = v, \\ \frac{dv}{dt} = -\omega_0^2 x. \end{cases}$$

In a finite difference form, the first step equation is

$$\begin{cases} \frac{x_{t+\Delta t/2} - x_t}{\Delta t/2} = v_t, \\ \frac{x_{t+\Delta t/2} - v_t}{\Delta t/2} = -\omega_0^2 x_t. \end{cases}$$

And the second step equation is

$$\begin{cases} \frac{x_{t+\Delta t} - x_t}{\Delta t} = v_{t+\Delta t/2}, \\ \frac{x_{t+\Delta t} - v_t}{\Delta t} = -\omega_0^2 x_{t+\Delta t/2}. \end{cases}$$

Assuming  $x_t = Ae^{-i\omega t}$ , we have the discrete-time dispersion relation for the 2nd-order Runge-Kutta method

$$(\omega\Delta t)^2 - 4\sin^2\left(\frac{\omega\Delta t}{2}\right) = -\frac{1}{4}(\omega\Delta t)^4 e^{i\omega t}.$$

Letting  $\omega = \omega_0 + \delta\omega + i\gamma$ , we get

$$\frac{\gamma}{\omega} = \left(\frac{\omega\Delta t}{2}\right)^3.$$

This shows that, if we solve a pure oscillatory solution using the 2nd-order Runge-Kutta scheme, the mode has a numerical instability. Therefore,  $\omega\Delta t/2 \ll 1$  is needed for accuracy and stability.

### 2.2.6 Parallel computing

Parallel computing plays an important role in the gyrokinetic nonlinear simulation. In our work a simple MPI parallel computing scheme, the so-called domain cloning, has been adapted [35]. The simulation domain is cloned and each processing element (PE) has the same simulation domain. In this way, a copy of grid quantities can be broadcast to each of the clones. The particles are divided among the clones and each clone has its own set of particles. In the push phase of the simulation, each clone pushes its own set of particles. These particles reside only in their particular domain clone and never communicate with other domain clones. After charge deposition onto grids in a single clone, a global sum and broadcast are performed to get the total charge and current density array on each clone. Then, the grid calculation is replicated on each clone. The nonlinear simulation in our study has been carried out using 20 processors.

## 3 Linear benchmarking

### 3.1 Physical picture of linear growth of the mirror instability

*Thompson* gives a description of the growth of the mirror instability which corresponds to the traditional view of the MHD instability [6]. In his work, it shows that the perturbed perpendicular kinetic pressure induced by the compressible change of the magnetic field can be expressed as

$$\delta p_{\perp} = 2p_{\perp} \left( 1 - \frac{T_{\perp}}{T_{\parallel}} \right) \frac{\delta B}{B}. \quad (3.1)$$

It shows that whenever  $T_{\perp} > T_{\parallel}$ , the particle kinetic pressure decreases when the magnetic field pressure increases. The perturbed pressure in Eq. (3.1) is proportional to the unperturbed pressure. Therefore, when the unperturbed pressure is large enough, the total perturbed pressure caused by the field change could be opposite to the change of the magnetic pressure. This negative compression causes the mirror instability. For the Bi-Maxwellian distribution, the condition for the instability is

$$\delta p_{\perp} + \frac{B\delta B}{4\pi} < 0.$$

From Eq. (3.1), we can find the threshold condition for the mirror instability

$$\beta_{\perp} (T_{\perp}/T_{\parallel} - 1) > 1. \quad (3.2)$$

This MHD explanation of the mirror instability is incomplete. The pressure response in Eq. (3.1) is crucial to the instability, and the response of the particle pressure to the field is connected with magnetic “mirror force”. However, the “mirror force” is not the force in the normal sense as it does not change the total particle energy. The energy of particle only exchanges between perpendicular and parallel degrees of freedom by the mirror force. We shall see that the instability occurs through wave-particle resonance.

*Southwood* and *Kivelson* provide a kinetic model to explain the linear growth of mirror instability by using the so-called quasi-hydrodynamic theory [11]. Firstly, they write the perturbed distribution function of the particles as

$$\delta F = -\delta W_{\parallel} \frac{\partial F}{\partial W_{\parallel}} - \delta W_{\perp} \frac{\partial F}{\partial W_{\perp}} = \left[ \frac{\delta W}{T_{\parallel}} + \frac{\mu \delta B}{T_{\perp}} \left( 1 - \frac{T_{\perp}}{T_{\parallel}} \right) \right] F.$$

Here,  $W$ ,  $W_{\parallel}$ ,  $W_{\perp}$  are the total, parallel and perpendicular energy,

$$\delta W_{\parallel} = \delta W - \mu \delta B, \quad \delta W_{\perp} = \mu \delta B.$$

In the low-frequency limit,  $dW/dt = \mu \partial B / \partial t$ , for a perturbation varying as  $\exp(i\mathbf{k} \cdot \mathbf{r} + \gamma t)$ , we find

$$\delta F = \left[ \frac{\mu \delta B}{T_{\perp}} \left( 1 - \frac{T_{\perp}}{T_{\parallel}} \right) \right] F + \left( \frac{\gamma \mu \delta B}{\gamma + ik_{\parallel} v_{\parallel}} \right) \frac{F}{T_{\parallel}}.$$

The last term comes from the wave-particle resonance. When  $\gamma$  is small, this term is negligible except for the resonant particles with  $v_{\parallel} \approx 0$ . It shows that the behavior of the resonant particles, which resonate with the wave, is much different from the rest of population in the distribution function. Their presence causes a difference in the dispersion relation of the mirror mode between the MHD and kinetic approaches. Taking the second moment of  $\delta F$  and substituting it to the perpendicular force balance equation yields

$$\frac{B \delta B}{4\pi} + 2p_{\perp} \left( 1 - \frac{T_{\perp}}{T_{\parallel}} \right) \frac{\delta B}{B} + 2 \frac{\gamma}{k_{\parallel}} \left( \int dv_{\parallel} \pi \delta(v_{\parallel}) F_{\parallel} \right) \frac{T_{\perp}^2}{T_{\parallel}} \frac{\delta B}{B} = 0, \quad (3.3)$$

where  $F_{\parallel}$  is the distribution function after the integral over the perpendicular velocity has been carried out. The Eq. (3.3) represents the total perpendicular pressure balance. The first term on the left hand side is the perturbed magnetic pressure, the second term is the adiabatic response of the bulk plasma to the magnetic perturbation and the third term represents the response of the resonant particles with very slow parallel velocity. Unlike what occurs for the bulk of the plasma where energy is simply exchanged between perpendicular and parallel degrees of freedom, the energy of resonant particles does change when the instability develops. Since  $v_{\parallel} \approx 0$ , the resonant particles do not move a significant distance along the field in the instability growth time ( $1/\gamma$ ). Thus the change of field acting on a resonant particle is simply due to the local temporal increase or decrease of field. In contrast, for the bulk of the plasma, the predominant change of field acting on the particle is from the spatial variation of the field perturbation and due to the particle motion in the field.

The linear mirror instability thus progresses in the following way. The field increase/decrease leads to a pressure decrease/increase in the bulk plasma that causes a net local pressure deficit/surplus. The pressure is balanced by the resonant particle pressure. The resonant particles are accelerated/decelerated by the increasing/decreasing field thus resulting in an anti-phase compared to the bulk of plasma.

However, because of the limitation of the quasi-hydrodynamic theory, *Southwood* and *Kiverson* do not consider the effects of finite Larmor radius to the linear growth rate. By using the gyrokinetic theory, we have discussed the FLR effects to the growth rate of the mirror instability [28].

### 3.2 Linear simulation and benchmark

To verify the simulation code, we carry out a linear simulation and compare the simulation results to our analytical results [28]. By using the gyrokinetic equations and the perpendicular Ampere's law introduced in Section 2, a 1D gyrokinetic simulation code is developed. Here, we assume  $\mathbf{k} = (k_{\perp}, 0, k_{\parallel})$  in XOZ plane,  $k_{\perp}$  along  $x$ -direction,  $k_{\parallel}$  along  $z$ -direction, and the ambient magnetic field points to  $z$ -direction. In the linear simulation, by using the  $\delta f$  scheme and keeping only the first order terms of small quantity  $\varepsilon$  used in the gyrokinetic approximation Eq. (2.1), we can solve the linear gyrokinetic equation from Eq. (2.2) by integrating along the unperturbed orbits. The positions of ions in  $z$ -direction are needed to be advanced through equation of motion (2.3). Right hand sides of Eqs. (2.4)-(2.5) are zero for the 1D linear simulation. The perpendicular Ampere's law, Eq. (2.6), can be solved by using the fast Fourier transform (FFT) and taking  $\delta A_y = -i\delta B_{\parallel}/k_{\perp}$  in  $k$ -space.

In the linear run of this simulation code, only a single mode  $m = n = 1$  is calculated using a Fourier filter in  $k$ -space, where  $m$  and  $n$  is the mode number in perpendicular and parallel direction. Accordingly, the size of simulation box is chosen as  $L_x = 2\pi/k_{\perp}$  in the  $x$ -direction, and

$$L_z = L_x / (k_{\parallel} / k_{\perp})$$

in the  $z$ -direction. The simulation domain is discretized by a set of grids in both  $x$  and  $z$  directions and the positions of ions are loaded uniformly in the cells with the Bi-Maxwellian distribution in the velocity space.

In the Vlasov-Maxwell equations, all the physical quantities have their own physical units. This is not convenient for simulation. Therefore, all the time quantities are normalized by ion Larmor frequency  $\Omega_i$  and the length quantities by ion Larmor radius  $\rho_i$ . As a result, the velocity quantities are normalized by ion perpendicular thermal velocity  $v_{i,\perp} = \Omega_i \rho_i$ . Thus, the normalized simulation box length are

$$\hat{L}_x = 2\pi / (k_{\perp} \rho_i), \quad \hat{L}_z = \hat{L}_x / (k_{\parallel} / k_{\perp}).$$

To make sure that the numerical resolution does not affect the physics, we have carried out convergence studies with regard to the number of particles  $N_p$ , the number of grids  $N_g$  and the size of time step  $\Delta t \cdot \Omega_i$  [28]. In our simulation, we choose  $N_p = 1.6 \times 10^5$ ,  $N_g = 64$  per mode and the normalized time step  $\Delta t \cdot \Omega_i = 1$  to insure that uncertainty is less than 3% [28].

The code is benchmarked by comparison between the linear growth rates obtained from simulation and corresponding analytical solutions [28]. In Fig. 2, for  $\beta_{i,\perp}$  and  $A_i = 1$ ,

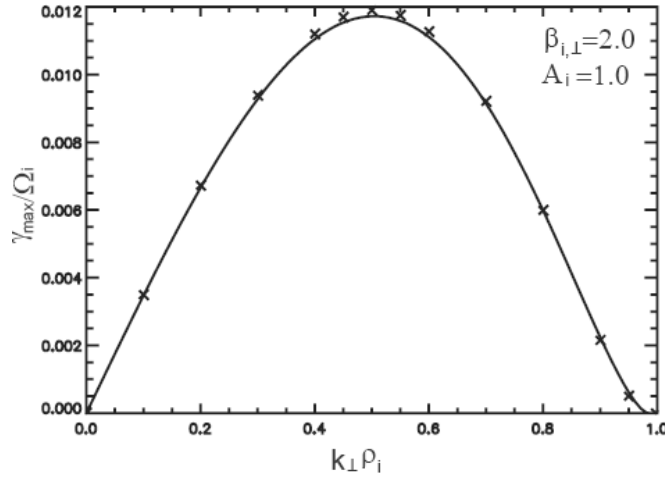


Figure 2: Maximum growth rate of the mirror instability obtained from 2D linear gyrokinetic simulation in uniform plasma. For comparison, the solid line is the corresponding analytic result from gyrokinetic theory.

the crosses indicate the results from linear simulation and the solid line indicates the results from the theoretical analysis based on the linear gyrokinetic theory. It shows that the numerical results agree very well with the theoretical prediction. Therefore, this linear simulation recovers the analytic theory of the mirror instability, and the benchmark provides a linear verification of the simulation code for the nonlinear simulation.

## 4 Nonlinear simulation results

*Kivelson and Southwood* [12] present a simple nonlinear saturation model of the mirror instability by using the theory of the relaxation to a marginal stability. In their work, the particles can be divided to the trapped particles with large pitch angle and untrapped particles with small pitch angle. In the part of the perturbation where the field increases, the trapped particles will be excluded from the rising field region by the mirror force. This produces a decrease in the particle pressure and thus allows the marginally stable state to be achieved. In the center of magnetic field well, although no particle can be excluded, some trapped particles can be cooled by losing perpendicular energy through betatron deceleration as

$$\Delta W = \mu \Delta B = W_{\perp} (\Delta B / B).$$

In this way, the perpendicular particle pressure decreases, the growing mirror perturbation in the field well can be stabilized by the relaxation to a marginal stability. We now use our gyrokinetic PIC code to study the nonlinear saturation of the mirror instability.

Building on the linear benchmark of the gyrokinetic simulation of the mirror instability in Section 3, we can perform the nonlinear simulation. In the nonlinear simulation, by using the  $\delta f$  method and keeping the second order terms of small quantity  $\varepsilon$ , we can solve

the nonlinear gyrokinetic Vlasov equation from Eq. (2.2). The velocity and acceleration of ions in the  $z$ -direction can be advanced through the equations of motion Eqs. (2.3)-(2.5). Here, the nonlinear effect from the parallel acceleration, which is a second order small quantity, is considered in the gyrokinetic equation. Combined with the perpendicular Ampere's law (2.6), they are the Vlasov-Maxwell equations for the nonlinear gyrokinetic simulation.

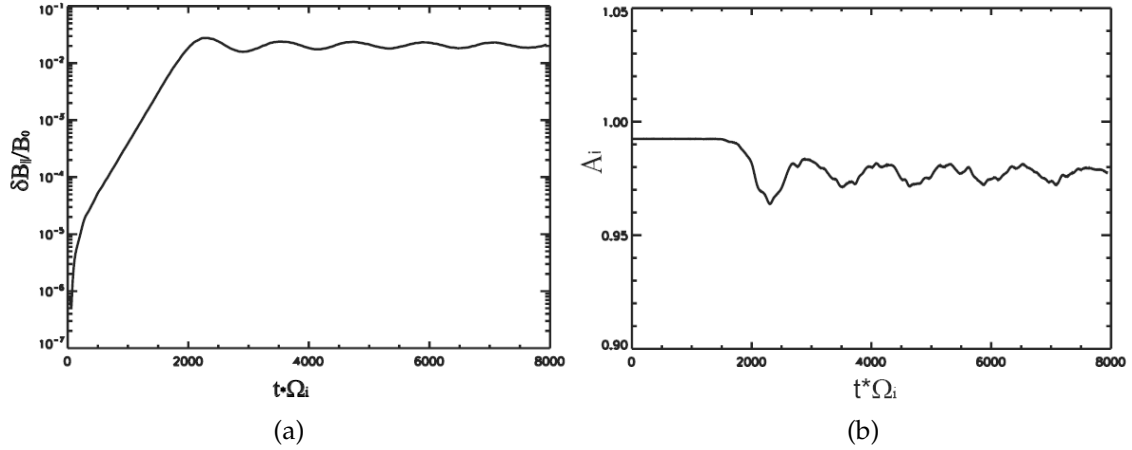


Figure 3: Time history of the perturbed parallel magnetic field and temperature anisotropy for  $\beta_{i,\perp} = 2$  and  $A_i = 0.99$ .

Before initiating the complicated nonlinear study of the mirror turbulence, the simple nonlinear simulation of a single mode needs to be carried out. Here, we use  $\beta_{i,\perp} = 2$  and  $A_i = 0.99$ ,  $k_{\perp}\rho_i = 0.2$ ,  $k_{\parallel}/k_{\perp} = 0.2$ . Fig. 3a shows the time history of the amplitude of the perturbed parallel magnetic field. The linear growth and nonlinear saturation of the mirror mode are indicated in the early part of this graph. Then it shows that the amplitude of the saturated mode oscillates in time and the oscillation period is  $\hat{t}_{nl} = t_{nl} \cdot \Omega_i \approx 1170$ , i.e.,

$$\hat{\omega}_{nl} = \omega_{nl} / \Omega_i \approx 0.0054.$$

From Fig. 3a, we find that  $\delta B_{\parallel} / B_0 \approx 0.023$  after saturation. From the motion equation of the deeply trapped particles driven by parallel mirror force,

$$m\ddot{x} = -\mu\nabla_{\parallel}\delta B,$$

we can calculate the bounce frequency of the trapped particles under such amplitude of the perturbed magnetic field

$$\hat{\omega}_b = \hat{\omega}_b / \Omega_i = \left( k_{\parallel}^2 \frac{\mu B_0}{\Omega_i^2} \frac{\delta B_{\parallel}}{B_0} \right)^{1/2} = \frac{k_{\parallel}}{k_{\perp}} k_{\perp} \rho_i \sqrt{\frac{\delta B_{\parallel}}{2B_0}} = 0.0043. \quad (4.1)$$

According to the parameters adopted and the linear simulation result, we also know that the linear growth rate of this mode is  $\hat{\gamma} = \gamma / \Omega_i \approx 0.0043$  which matches well with our

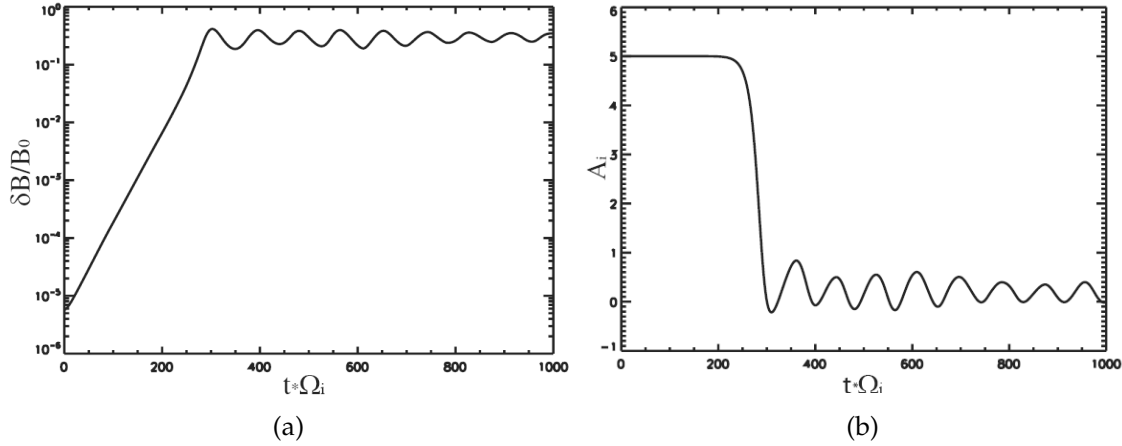


Figure 4: Time history of the perturbed parallel magnetic field and temperature anisotropy for  $\beta_{i,\perp} = 12$  and  $A_i = 5$ .

analytical result from the linear gyrokinetic theory [28],

$$\hat{\gamma} = \frac{k_{\parallel}}{k_{\perp}} k_{\perp} \rho_i \frac{-\Lambda + \beta^* A_i}{\sqrt{\pi} \beta^* (1 + A_i)^{3/2}}, \quad (4.2)$$

where

$$\Lambda = 1 + \frac{k_{\parallel}^2}{k_{\perp}^2} [1 + \alpha_b (\beta_{\perp} - \beta_{\parallel})], \quad \beta_{\perp}^* = \beta_{\perp} e^{-k_{\perp}^2 \rho_i^2 / 2} [I_0(k_{\perp} \rho_i) - I_1(k_{\perp} \rho_i)].$$

We find that the nonlinear oscillation frequency of the mirror mode is close to the bounce frequency of the trapped particles and the linear growth rate of the mode,

$$\hat{\omega}_{nl} \sim \hat{\omega}_b \sim \hat{\gamma}. \quad (4.3)$$

At the same time, in Fig. 3b, it shows that the temperature anisotropy almost does not change when saturation happens. This means that the mechanism of the relaxation to the marginal stability does not work in the nonlinear saturation of mirror mode in this case. Rather, it is the phase space trapping that determines the nonlinear saturation process of the mirror mode. This saturation mechanism for mirror mode has not been mentioned before.

However, for the strong drive case, in which  $\beta_{i,\perp}$  and  $A_i$  are much larger than 1, the situation is different. From Figs. 4a and 4b, for  $\beta_{i,\perp} = 12$  and  $A_i = 5$ , it shows that the temperature anisotropy drops dramatically to zero after saturation. It is consistent with the previous study using the marginal stability theory as discussed in Section 4.1 [12, 13]. Therefore, we find that there may be two different types of saturation mechanisms for the mirror instability. The phase space trapping plays a dominant role for the weak drive and the mechanism of the relaxation to the marginal stability is dominant for the strong drive.

## 5 Summary

In this paper, we have presented a gyrokinetic PIC model for the linear and nonlinear simulation of the compressional mirror instability. Our linear gyrokinetic particle simulation results agree with the analytical results very well and it provides a good benchmark for the nonlinear simulation. From the difference of nonlinear simulation results of mirror mode under different conditions, we find that there are different dominant saturation mechanisms. For the weak drive case, the mechanism of the phase space trapping is dominant. However, the mechanism of the relaxation to the marginal stability is dominant for the strong drive case.

## Acknowledgments

This work is supported by the US Department of Energy (DOE) Grant DE-FG02-07ER54916 and by a NSF CAREER Award, Grant No. ATM-0449606.

## References

- [1] W. W. Lee, *J. Comput. Phys.* 72 (1987) 243.
- [2] Z. Lin, T. S. Hahm, W. W. Lee, W. M. Tang, R. B. White, *Science* 281 (1998) 1835.
- [3] Z. Lin, L. Chen, *Phys. Plasmas* 8 (2001) 1447.
- [4] W. W. Lee, J. L. V. Lewandowski, T. S. Hahm, Z. Lin, *Phys. Plasmas* 8 (2001) 4435.
- [5] L. I. Rudakov, R. Z. Sagdeev, *Dokl. Akad. Nauk SSSR, Engl. Transl.* 6 (1961) 415.
- [6] W. B. Thompson, *An Introduction to Plasma Physics*, (2nd ed.), Oxford Pergamon, New York 1964, p. 216.
- [7] M. Tajiri, *J. Phys. Soc. Jpn.* 22 (1967) 1482.
- [8] A. Hasegawa, *Phys. Fluid* 12 (1969) 2642.
- [9] O. A. Pokhotelov, R. A. Treumann, R. Z. Sagdeev, et al, *J. Geophys. Res.* 107(A10) (2002) 1312.
- [10] O. A. Pokhotelov, R. Z. Sagdeev, M. A. Balikhin, R. A. Treumann, *J. Geophys. Res.* 109 (2004) A09213.
- [11] D. J. Southwood, M. G. Kivelson, *J. Geophys. Res.* 98 (1993) 9181.
- [12] M. G. Kivelson, D. J. Southwood, *J. Geophys. Res.* 101 (1996) 17365.
- [13] F. G. E. Pantellini, *J. Geophys. Res.* 103 (1998) 4789.
- [14] W. Allan, E. M. Poulter, E. Nielsen, *J. Geophys. Res.* 87 (1982) 6163.
- [15] A. D. M. Walker, E. Nielsen, *J. Geophys. Res.* 87 (1982) 9135.
- [16] K. Takahashi, C. T. Russell, R. A. Anderson, *Geophys. Res. Lett.* 12 (1985) 613.
- [17] K. Takahashi, C. Z. Cheng, R. W. McEntire, L. M. Kistler, *J. Geophys. Res.* 95 (1990) 977.
- [18] E. A. Lucek, M. W. Dunlop, et al, *Ann Geophysicae* 17 (1999) 1560.
- [19] E. A. Lucek, M. W. Dunlop, et al, *Ann Geophysicae* 19 (2001) 1421.
- [20] F. Sahraoui, et al, *Phys. Rev. Lett.* 96 (2006) 075002.
- [21] D. E. Huddleston, R. J. Strangeway, X. Blanco-Cano, et al., *J. Geophys. Res.* 104 (1999) 17479.
- [22] N. Andre, G. Erdos, M. Dougherty, *Geophys. Res. Lett.* 29(20) (2002) 1980.
- [23] S. P. Gary, *J. Geophys. Res.* 97 (1992) 8519.
- [24] J. R. Johnson, C. Z. Cheng, *J. Geophys. Res.* 102 (1997) 7179.

- [25] P. Hellinger, Phys. Plasmas 14 (2007) 082105.
- [26] E. A. Frieman, L. Chen, Phys. Fluids 25 (1982) 502.
- [27] A. Brizard, J. Plasma Phys. 41 (1989) 541.
- [28] H. Qu, Z. Lin, L. Chen, Phys. Plasmas 14 (2007) 042108.
- [29] C. Z. Cheng, J. R. Johnson, J. Geophys. Res. 104 (1999) 413.
- [30] L. Chen, S. Tsai, Plasma Phys. 25 (1983) 349.
- [31] C. K. Birdsall, A. B. Langdon, Plasma Physics via Computer Simulation, Adam Hilger, Bristol 1991.
- [32] S. E. Parker, W. W. Lee, Phys. Fluids B 5(1) (1993) 77.
- [33] G. Hu, J. A. Krommes, Phys. Plasmas 1 (1994) 863.
- [34] W. H. Press, et al, Numerical Recipes, Cambridge University Press, Cambridge 1992.
- [35] C. Kim, S. E. Parker, J. Comput. Phys. 161 (2000) 589.